IOP Publishing New J. Phys. 25 (2023) 123015 https://doi.org/10.1088/1367-2630/ad0e8b

New Journal of Physics
The open access journal at the forefront of physics

Deutsche Physikalische Gesellschaft DPG
IOP Institute of Physics

Published in partnership with: Deutsche Physikalische Gesellschaft and the Institute of Physics

OPEN ACCESS

RECEIVED
20 July 2023

REVISED
7 November 2023

ACCEPTED FOR PUBLICATION
21 November 2023

PUBLISHED
8 December 2023

PAPER

Ultrashort Ne^+ ion pulses for use in pump–probe experiments: numerical simulations

P Kucharczyk, A Golombek, M Schleberger, A Wucher and L Breuer*

Fakultät für Physik, Universität Duisburg-Essen, D-47057 Duisburg, Germany
* Author to whom any correspondence should be addressed.

E-mail: lars.breuer@uni-due.de

Keywords: ion pulses, pump-probe, numerical simulations

Abstract

A time resolved experiment to investigate the ultrafast dynamics following an ion impact onto a solid surface requires an ultrashort ion pump pulse in combination with a properly synchronized and time resolved probe. In order to realize such an experiment, we have investigated a strategy to use femtosecond laser photoionization of atoms entrained in a pulsed supersonic jet for the production of sufficiently short ion pulses. While the generation of Ar^{q+} ions was targeted in previous work, it has in the meantime been demonstrated that argon is not suitable due to extensive cluster formation in the supersonic expansion. Here, we therefore present numerical simulations investigating the use of neon as a precursor gas and show the feasibility of pulses containing up to ∼1000 Ne^+ ions at keV energies and picosecond duration. In the process, we demonstrate that space charge broadening can be significantly reduced by detuning the flight time focusing conditions of an ion bunching system. Moreover, the results show that a controlled variation of the buncher geometry and potentials permits the generation of picosecond pulses at variable ion energy between 1 and 5 keV.

1. Introduction

Ion-surface and solid interactions form the foundation of various material modification techniques and analysis methods. Techniques such as focused ion beam milling and defect engineering exploit this principle, as do analysis methods such as secondary ion mass spectrometry. Although these tools have been known for decades, they continue to be subjects of ongoing development and state-of-the-art research. During the interaction of a charged particle with a solid, processes depend on factors like kinetic energy, which relates to the nuclear and electronic stopping of the projectile in the target, and potential energy linked to the charge of the ion. Energy transferred from the projectile excites the target's electrons and nuclei. This results in ionization along the projectile's path, creation of non-equilibrium states, and formation of phonons, defects, and voids. Moreover, the implanted projectile ion further alters the solid's structure. Crucially, these interactions occur in the ultrafast time domain, demanding specialized investigation methods. To follow ultrafast dynamics in solids, i.e. excitation by laser radiation, pump probe schemes have been used with great success [1–6]. These schemes are widely used to directly follow the relaxation of excitation events in the time domain with a temporal resolution of (sub-) picoseconds. To date, there are no comparable experiments to follow the dynamics triggered by the impact of an energetic particle onto a solid surface. The time scales involved in this case are very similar to those for laser excitation. Such a particle, typically an ion, transfers its kinetic energy rapidly (on as—fs time scales) and very locally to the nuclei and electrons of the target, creating an extreme non-equilibrium state. All available information about the equilibration of these states rely on computer simulations and theoretical approaches, which currently can only be experimentally verified by measuring the asymptotic final state. These leads to assumptions and simplifications justified only by the correct description of observables characterizing the state of the experiment rather long times after the impact, such as sputter yields, electron yields, or angular and energy distributions of emitted particles (atoms, electrons or photons). The temporal dynamics of the underlying atomistic processes has not yet been

directly accessible by experimental measures. One can imagine probing these underlying processes directly by using the same pump–probe approach as used for investigating other ultrafast dynamics in solids. The challenge here is to produce an ultra-short ion pulse as a pump that must be jitter-free synchronized with a probe pulse, i.e. a femtosecond laser pulse and a well-known impact time onto the target surface.

While the hurdle of generating ultra-short ion pulses is considerable, it is just one of many challenges to address. A significant issue in using charged particles as pump or probe pulses is the inherent Coulomb repulsion. This repulsion induces pulse broadening and alters the momentum of particles within the pulse package. This effect is less important when using electrons due to their higher velocities and shorter interaction times, it however profoundly influences the feasibility of creating ultra-short ion pulses, especially with higher charge states of the ions. Such intrinsic challenges are accompanied by technical difficulties. For instance, while numerical simulations may manage these complexities, real-world experiments present formidable obstacles. To mitigate the effects of repulsion, the experimentally realized ion flight region must be highly compact, which in turn restricts access for detectors and probes.

Additionally, choosing the right properties to probe in ion-based pump–probe experiments, presents its own set of challenges. In typical optical or electron-based pump–probe experiments, the focus is on observing the post-stimulation disappearance and subsequent return of a signal. When considering ions, their primary interaction region will be typically relatively small, while an optical probe or pump affects the entire sample. To enhance the excited sample size, numerical simulations are vital for pinpointing parameters that may allow to augment the number of ions per primary pulse. Yet, we must identify observables, that manifest only when both the ion and optical pulses overlap within their respective interaction times. A potential property to explore might be the lifetime of the electronic excitation initiated by the ion pulse via the photo-effect. Here, a sub-threshold laser pulse could probe the sample, i.e. only electrons from the ion-excited hot regions would be emitted.

Recognizing these challenges and the immense potential of the method, research teams have ventured into designing appropriate solutions [7] and have developed different strategies to produce the necessary short ion pulses [8–10], involving acceleration in laser driven plasmas or so-called neutralized drift compression techniques [11]. These approaches led to light ions (H and He) with kinetic energies of 1–10 MeV [12]. When these ions collide with a solid surface at such energies, the energy transfer process is completely dominated by electronic stopping, leading to an energy transfer from the ion to the electronic system of the target comparable to laser excitation. Since most applications of ion beams operate with heavy ions in the range of nuclear stopping, where the initial pulse leads to a collisional cascade of mostly elastic collisions, this energy range is of great interest. Therefore, ultrashort ion pulses with keV energies are needed. While bunching techniques generally allow to produce short ion pulses down to several ten picoseconds in that regime, these pulses yield broad energy spectra due to the bunching process. Therefore, we have proposed an approach using femtosecond strong field-ionization of ultracold atoms from a supersonic neutral gas jet [13]. Earlier experiments utilizing argon at room temperature as a process gas have demonstrated pulse widths on the order 180 ps for keV Ar^{q+} ions. The main limiting factor for the pulse width in this case was thermal broadening due to the thermal motion of the argon atoms prior to the ionization event. While cooling of the argon gas is in principle possible, it yields complications in our experimental approach. Adiabatic expansion of argon into vacuum leads to extensive cluster formation and is used in many commercial ion sources to produce gas cluster ion beams. While these applications rely on the formation of such gas clusters, cluster formation is unwanted in our experimental approach since the energy release after the ionization event counteracts the supersonic cooling effect. The experiment has therefore now been switched to neon as a precursor gas, and we have demonstrated the generation of Ne^{+} ion pulses from a supersonic beam which are significantly shortened as compared to those produced by room temperature background gas [14], by calculating the temporal pulse width from the thermal broadening of the pulse to (18 ± 4) ps. However, the directly experimentally measured pulse width of about 135 ps is now limited by the time resolution of the currently used ion detection system, thereby generating the need to perform numerical simulations for this system in order to investigate the prospects of the method.

Due to the greater ionization potential of neon compared to argon, we expect different spatial ionization profiles as well as different space charge interactions as compared to our previous simulations. Additionally, both atom species differ in the rebound momentum induced by the liberated photoelectrons, resulting in different starting velocity distributions of the ions immediately after photoionization. For that reason, it is not possible to directly rescale the results of numerical simulations performed previously for argon ions just in terms of the different ion mass [15]. In order to correctly predict the arrival time distribution for neon ions, one has to specifically model the photoionization process in the same way as done in [14, 15] for argon. For situations where more than one ion is produced per laser shot, the spatial distribution of the resulting ion clouds must be included in the following ion trajectory simulations in order to account for the coulomb

interaction within the generated ion bunch. In addition to the strategy to mitigate space charge induced broadening in such situations by blowing up the effective ionization volume [15], we present a technique to further reduce this effect by a controlled detuning of the flight time focusing conditions in the ion bunching system, thereby allowing the generation of picosecond pulses containing more than 1000 Ne^+ ions at 5 keV energy. Moreover, we will show that a controlled *in-situ* variation of the buncher geometry along with its electrode potentials allows to tune the ion energy down to about 1 keV without sacrificing the time resolution.

2. Simulations

The computational methods mimic an experimental setup designed to create ultra-short ion pulses and perform pump–probe experiments based on ion irradiation of sample surfaces and were already described in great detail in [13, 15] and will only be repeated in a general way here. The experimental setup consists of 3 electrodes which are arranged plan parallel as shown in figure 1 (left panel). This arrangement is called ion buncher and comprises of 2 sections. The first section between Electrode 1 and 2 is used to generate the ion bunches from a supersonic, geometrically cooled gas beam. The cooling is not included in the simulations presented here, we just assign a certain temperature distribution as described later in this manuscript. The ionization of the neutral gas atoms is performed via strong field ionization in an intense laser field of power densities up to 10^{17} W cm^{-2} at a wavelength of 800 nm and pulse widths of 50 fs. To reach these densities the laser beam used in the experiment needs to be tightly focused into the gap between the first two electrodes. The power of the laser in the simulations is adjusted to create the desired number of ions per bunch from the cold neutral gas beam.

The ion bunches created in this gap are accelerated towards electrode 2 by an electrical field applied between electrode 1 and electrode 2 and transmitted through an 80 μm hole in electrode 2 to the second section of the buncher. The diameter of the hole was chosen to mimic the experimental setup, in which the diameter was chosen as small as possible. The 80 μm are a trade-off between the technical possible and the physical requirement not to distort the electrical field within the buncher. The thickness of the middle electrode is set in the simulations to be $D_2 = 100$ μm. These geometrical restrictions are confining the effective sensitive volume of the ionization process and are therefore an additional limiting factor for the number of usable ions that can be transmitted through the hole in electrode 2 into the second section of the ion buncher. Ions that are created outside the sensitive volume are neglected for the further simulation (compare figure 1 (right panel)). The ion bunch is than further accelerated by the field applied between electrode 2 and 3 towards electrode 3 which acts as target. The detected and analyzed ion pulse in the simulations presented here consists of all ions reaching the surface of electrode 3.Previous works of our group [14, 15] have described the details of the trajectory simulations in great detail and will only be reported in a very general manner here. The fundamental of the simulations is the boundary element method implemented in the 'Charged Particle Optics' software package [16–18]. The initial results generated by that package are treated in a similar way as in the SIMION [19] code. Therefore, the results are refined in the central region surrounding the ion-optical axis using a finite difference approach. In a next step the 'General Particle Tracer' [20–23] package is used to further follow the ion trajectories. This package simulates the trajectories within a static electrical field, i.e. the influence of the space charge generated by the flying ion bunch on the electric field was neglected. The ionization probability for the neutral gas particles in the laser field was derived from theory developed by Ammosov, Delone and Krainov (theory) [24], delivering probability distributions for the ionization states of the irradiated particles from 0 (neutral) to n. From these distributions the starting positions and charged states of the photo ions were chosen statistically and the according starting velocities were selected from a thermal distribution at a given temperature $T_{\mathrm{Start}} = (T_{\parallel}, T_{\perp})$, where $T_{\parallel}$, $T_{\perp}$ describe the velocity distributions parallel and perpendicular to the propagation direction of the gas beam, respectively. From experimental data [25] we set $T_{\parallel} = 500$ mK and $T_{\perp} = 280$ mK. The drift velocity due to the gas expansion $v_{\parallel}$ was assumed as $v_{\parallel} = 770$ m s^{-1}, again derived from corresponding experimental data [25].

Within such an ion bunch all trajectories were run into parallel and the full coulombic interaction between the individual ions was taken into account during the calculation. Again, for the results only such ions were counted, that made their way through the whole in electrode 2. The time-of-flight when hitting the surface of electrode 3 was than histogrammed with typical bin widths of 20 fs. In order to assess the temporal pulse width, the resulting histograms are plotted versus the deviation from the most probable ion arrival time ('relative flight time').

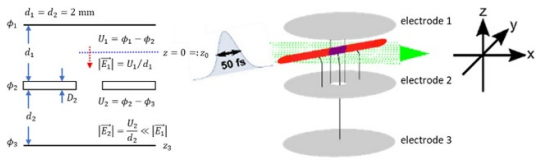

Figure 1. Left: simulation volume of the ion optical buncher consisting of two (nearly) homogeneous electric fields $\vec{E}_1$, $\vec{E}_2$ between electrodes 1 & 2 and 2 & 3, respectively. Middle: sketch of the total ionization volume (bright shaded, red) and the volume from which the ions contributing to the pulse reaching the target electrode 3 must originate (dark shaded, purple), green dotted lines indicate the Ne atoms entrained in the supersonic jet. right: The coordinate system used in this paper.

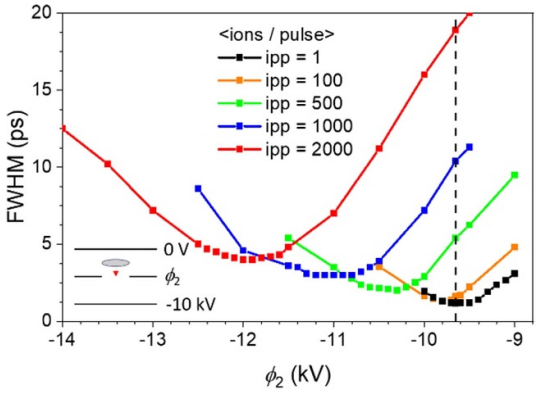

Figure 2. FWHM of flight time distributions calculated for Ne^+ ion pulses containing a variable number of ions per pulse. The data were generated assuming an astigmatic laser beam ($w_{0x} = 72$ μm, $w_{0z} = 15.25$ μm) and a gas beam density of 10^{17} m^{-3}. The laser intensity I_0 is being adjusted to deliver the desired number of ions. The dotted line represents the flight time focus for single particle pulses, which is the minimum reachable pulse width.

3. Results and discussion

The coordinate system used in the remainder of this paper is shown in figure 1 (right panel). The supersonic beam and laser beam propagate in x- and y- direction, respectively, and the photo-ions are accelerated in (negative) z-direction.

3.1. Optimizing electric fields

In [15] we have shown that space charge broadening can be significantly reduced by using an astigmatic laser beam profile for photoionization of the atoms entrained in the gas jet. In this chapter we present a technique to further reduce space charge broadening by a controlled detuning of the flight time focusing conditions. Assuming the potentials $\phi_1 = 0$ V and $\phi_3 = -10$ kV for the electrodes 1 and 3, the potential ϕ_2 at the center electrode 2 is normally fixed by the requirement to ensure first order flight time focusing conditions for ions generated in the center between electrodes 1 and 2 at the position of the target surface 3. For ion pulses containing only one single ion, this configuration results in the temporally narrowest ion arrival time distribution. In this case, the ion 'pulse width' is determined by the full width at half maximum (FWHM) of this distribution. The picture changes if one increases the number of ions per pulse, for instance by increasing the laser intensity. In this case, the space charge interaction between the ions results in a significant broadening of the ion arrival time distribution. The temporal width (FWHM) of ion pulses containing a variable number of ions is shown as a function of the potential ϕ_2 of the center electrode figure 2. Under 'normal' conditions, this potential would be kept fixed at the value of $\phi_2 = -9652.5$ V, which ensures first order flight time focusing conditions for single ions starting around the center of the effective ionization volume (indicated by the dotted line). It is evident that this would lead to an extensive broadening of the pulse if the number of ions is increased.

On the other hand, a controlled detuning of the flight time focusing conditions via variation of ϕ_2 can obviously reduce this effect. The optimum value of ϕ_2, leading to the temporally shortest ion pulses, depends on the number of ions per pulse and shifts with increasing number of ions. As seen from figure 2, the duration of pulses containing 2000 ions can be reduced by about 75% down to about 4 ps using this strategy. The reason for the apparent re-compression of the pulse by deviating from first order flight time focusing conditions becomes more clear in figure 3, which shows the flight time distributions of the ions calculated for this example in the top row along with the corresponding distribution of their starting positions in the

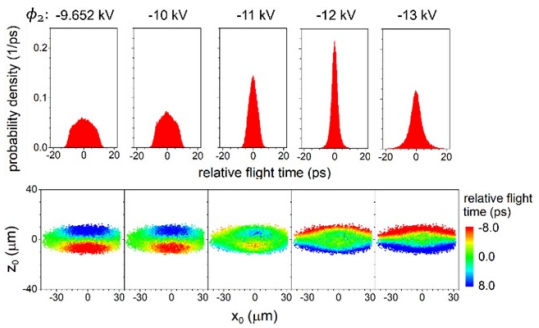

Figure 3. (Top) Relative flight time distributions calculated for Ne^+ ions within a pulse containing on average 2000 ions at different values of the potential ϕ_2. (Bottom) Flight time of ions reaching the target electrode 3 vs. starting position in the *xz*-plane located 3.1 mm above electrode 3 corresponding to the flight time distributions depicted in the top row.

plane perpendicular to the laser propagation axis (bottom row). In order to visualize the space charge influence, each starting position is colored by the respective relative ion flight time for different potentials ϕ_2. Under first order flight time conditions ($\phi_2 = -9652.5$ V), single ions which start at the center of the effective ionization volume would exhibit the shortest flight time, while ions starting on either side away from this point would exhibit the same flight time deviation ('flight time focusing'). If the ion packet contains more than one ion, on the other hand, ions starting on the side closer to the target electrode 3 are additionally accelerated along the extraction direction by the space charge of the ion cloud, thereby leading to shorter flight times, while ions generated further away from electrode 3 are accelerated in the opposite direction, thus leading to longer flight times. This correlation between ion velocity and starting position within the travelling ion packet can be utilized in order to at least partly mitigate the influence of space charge broadening via a controlled detuning of the flight time focusing properties. More specifically, the variation of ϕ_2 generates a flight time dispersion as a function of starting position along the extraction axis which is opposed to the space charge induced dispersion. This way, it is possible to realize pulses containing more than 10^3 ions at pulse durations of several picoseconds as shown in figure 2. A further variation of ϕ_2 finally overcompensates the space charge effects, resulting in the fact that the ions generated closer to electrode 3 become the slowest ions in the bunch. The corresponding flight time distribution of the ion pulses is shown in the top row of figure 3, illustrating the effect of counteracting space charge induced pulse broadening by appropriate variation of ϕ_2.

3.2. Optimizing electrode distances

The temporal broadening of ion pulses due to their initial velocity distribution (parametrized by the temperature $T_\perp$) along the extraction field $\vec{E}_1$ can be estimated from the 'turn-around-time' difference of ions starting in opposite directions along the extraction axis as [25]:

$$\mathrm{FWHM}_{\mathrm{ions}}\left(\left|\vec{E}_1\right|\right) = \frac{2m}{q\cdot\left|\vec{E}_1\right|}\cdot\sqrt{2\cdot\ln(2)}\cdot\sqrt{\frac{k_B\cdot T_\perp}{m}} \propto \frac{1}{\left|\vec{E}_1\right|}.$$

According to this estimate the pulse length is determined by the electric field strength $\vec{E}_1$ between the top electrodes. Reducing the kinetic energy of the ions at the target electrode 3 by reducing the electric field strength $\vec{E}_1$ therefore leads to a broadening of the ion pulse $\propto 1/|\vec{E}_1|$. On the other hand, it would be desirable to reduce the kinetic impact energy of the ions without broadening the temporal pulse length. A possibility to generate such ion pulses is by adjusting the buncher as depicted in figure 4 (top). In this configuration, the potentials $\phi_1 = 0$ V, $\phi_2 = -10$ kV and the distance $d_1 = 2$ mm are fixed, resulting in a fixed extraction field $|\vec{E}_1| = 5$ kV mm^{-1}. As the ions are generated in the center of the electrodes 1 and 2, while the distance $d_{2^*} = D_2 + d_2$ is reduced, flight time focusing is possible if an appropriate electric field $\vec{E}_2$ is applied, which is opposed to $\vec{E}_1$. This way the electric field $|\vec{E}_1| = 5$ kV mm^{-1} leads to a strong compression of the ions between the electrodes 2 and 3, while $\vec{E}_2$ simultaneous deaccelerates the ions. This results in ion pulses with reduced kinetic energy at the target electrode 3. By varying the distance d_2 in the range 0.75 mm–2.0 mm, and adjusting the electric field $\vec{E}_2$ in order to ensure first order flight time focusing conditions at the target surface (similar to section 3.1), the resulting arrival time distribution of ions in pulses containing on average 10 ions are shown in figure 4 (bottom). It is seen that the pulse length attainable by this strategy is nearly constant around 1.2 ps and determined almost exclusively by the temperature $T_\perp$ parametrizing the ion velocity distribution along the extraction axis. A correlated change of the target

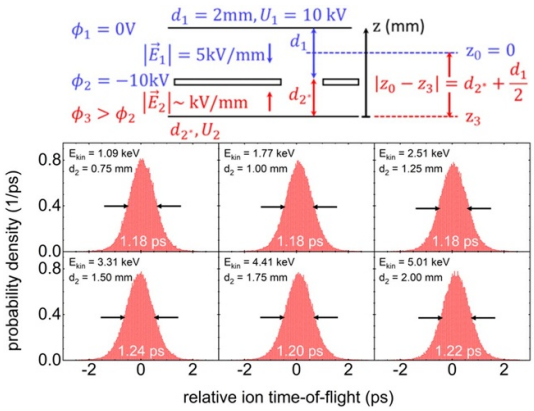

Figure 4. (Top) sketch of the simulated buncher geometry. Quantities during variation of d_{2^*} are depicted either blue (constant, while d_{2^*} is varied) or red (varied with d_{2^*}). (Bottom) relative flight time distributions for Ne^+ pulses containing 10 ions on average with different kinetic energies per ion. The parameter in the calculation were $I_0 = 5.1 \times 10^{14}$ W cm^{-2}, a laser focus diameter of 10 μm and a neutral gas density of 10^{17} atoms m^{-3}.

electrode potential along with a corresponding *in-situ* change of its position via, for instance, a motorized micrometer stage, would therefore open the possibility to continuously vary the ion energy in the range between 1 and 5 keV without any sacrifice to the picosecond pulse duration. A corresponding requirement for the experimental setup, namely the possibility to move electrode 3 while the experiment is running, is therefore incorporated in our new setup.

4. Conclusions

We present detailed ion trajectory simulations to calculate the arrival time distributions of Ne^+ ions generated via photoionization in a cold supersonic neon beam with full account of their generation, the resulting start configuration with respect to charge state, position and velocity distributions as well as the space charge broadening. In particular, we show that the generation of pulses containing from single up to several thousand ions with energies in the keV regime and picosecond duration is possible. By a controlled detuning of the flight time focusing conditions of the ion optical bunching setup, we found a useful method to counteract the effect of pulse broadening due to space charge effects. Moreover, the simulations reveal that it is possible to freely adjust the kinetic ion energy by appropriate adjustments of the buncher potentials and geometry.

In order to verify these predictions experimentally, it is necessary to improve the time resolution of our ion detection system from currently 135 ps [13]. For that purpose, we are working to replace the currently used microchannel plate ion detector by a streak technique delivering sub-picosecond resolution. Ultimately, it is planned to use the generated ion pulses in order to study the nuclear and electronic dynamics following an ion impact onto the target surface and compare the results with theoretical model calculations based, for instance, on molecular dynamics simulations. Possible probe strategies in such an ion pump–laser probe experiment include time resolved x-ray or electron diffraction, photoelectron emission or photoionization to study ion-induced order-disorder transitions, transient electronic excitations or nuclear collision and particle emission dynamics. The advantage of the laser-based ion pulse generation is that the laser-based probe can be optically synchronized with the ion impact without any electronic triggering jitter. We are confident that the strategy described here will therefore open path for a long missing experimental access to the ion-induced dynamics in solids.

Data availability statement

The data cannot be made publicly available upon publication because they are not available in a format that is sufficiently accessible or reusable by other researchers. The data that support the findings of this study are available upon reasonable request from the authors.

Acknowledgments

This work was funded by the Deutsche Forschungsgemeinschaft (DFG, German Research Foundation—Projektnummer 278162697—SFB 1242) in the frame of the Project ‘Exploring

Particle-Induced Excitations in the Time Domain' (C05) within the Collaborative Research Center (SFB) 1242 'Non-equilibrium dynamics in the time domain'.

ORCID iDs

M Schleberger https://orcid.org/0000-0002-5785-1186
A Wucher https://orcid.org/0000-0002-9244-9491
L Breuer https://orcid.org/0000-0002-7797-9662

References

[1] Von der Linde D, Sokolowski-Tinten K, Blome C, Dietrich C, Tarasevitch A, Cavalleri A and Squier J 2001 *Z. Phys. Chem.* **215** 1527
[2] Srinivasan R, Lobastov V A, Ruan C Y and Zewail A H 2003 *Helv. Chim. Acta* **86** 1761–99
[3] Rischel C, Rousse A, Uschmann I, Albouy P-A, Geindre J-P, Audebert P, Gauthier J-C, Fröster E, Martin J-L and Antonetti A 1997 *Nature* **390** 490–2
[4] Bauer M, Pawlik S and Aeschlimann M 1998 *Proc. SPIE - Int. Soc. Opt. Eng.* **3272** 201–10
[5] Bressler C and Chergui M 2004 *Chem. Rev.* **104** 1781–812
[6] Weisshaupt J, Rouzée A, Woerner M, Vrakking M, Elsaesser T, Shirley E and Borgschulte A 2017 *Phys. Rev.* B **95** 081101
[7] Aumayr F *et al* 2019 *J. Phys. B: At. Mol. Opt. Phys.* **52** 171003
[8] Schreiber J, Bolton P R and Parodi K 2016 *Rev. Sci. Instrum.* **87** 071101
[9] Dromey B *et al* 2016 *Nat. Commun.* **7** 10642
[10] Clark E L, Krushelnick K, Zepf M, Beg F N, Tatarakis M, Machacek A, Santala M I K, Watts I, Norreys P A and Dangor A E 2000 *Phys. Rev. Lett.* **85** 1654–7
[11] Seidl P A *et al* 2017 *Laser Part. Beams* **35** 373–8
[12] Senje L *et al* 2017 *Appl. Phys. Lett.* **110** 104102
[13] Breuers A, Herder M, Kucharczyk P, Schleberger M, Sokolowski-Tinten K and Wucher A 2019 *New J. Phys.* **21** 053017
[14] Kalkhoff L, Golombek A, Schleberger M, Sokolowski-Tinten K, Wucher A and Breuer L 2023 *Phys. Rev. Res.* **5** 033106
[15] Kucharczyk P, Golombek A and Wucher A 2020 *Nucl. Instrum. Methods Phys. Res.* B **483** 41–49
[16] Cubric D, Lencova B, Read F H and Zlamal J 1999 *Nucl. Instrum. Methods Phys. Res.* A **427** 357–62
[17] Read F H 2015 *Microsc. Microanal.* **21** 182–7
[18] Read F H and Bowring N J 2011 *Nucl. Instrum. Methods Phys. Res.* A **645** 273–7
[19] Dahl D A 2000 *Int. J. Mass Spectrom.* **200** 3–25
[20] De Loos M and Van Der Geer S 1996 *5th European Particle Accelerator Conf.* p 1241
[21] Van der Geer S 2003 The general particle tracer code: design, implementation and application
[22] Van der Geer S and De Loos M 1997 *Proc. 1997 Particle Accelerator Conf. (Cat. No. 97CH36167)* (IEEE) pp 2577–9
[23] Van Der Geer S B, Reijnders M P, De Loos M J, Vredenbregt E J D, Mutsaers P H A and Luiten O J 2007 *J. Appl. Phys.* **102** 094312
[24] Ammosov M V, Delone N B and Krainov V B 1986 *Sov. Phys - JETP* **64** 1191–4
[25] Moshammer R *et al* 2000 *Phys. Rev. Lett.* **84** 447